We are IntechOpen,
the world's leading publisher of
Open Access books
Built by scientists, for scientists

4,800
Open access books available

122,000
International authors and editors

135M
Downloads

Our authors are among the

154
Countries delivered to

TOP 1%
most cited scientists

12.2%
Contributors from top 500 universities

CLARIVATE ANALYTICS
BOOK CITATION INDEX
INDEXED
WEB OF SCIENCE™

Selection of our books indexed in the Book Citation Index
in Web of Science™ Core Collection (BKCI)

Interested in publishing with us?
Contact book.department@intechopen.com

Propagation of Shock Waves in Two Rooms Communicating Through an Opening

Isabelle Sochet, Kevin Gault and Luc Hakenholz

Abstract

Confined explosions represent a serious safety hazard as significant damage to humans and structures is observed, unlike in free-field explosions. An experimental small-scale study investigated the blast wave in a single-story building. The blast waves were generated by the detonation of a gaseous charge. The building was divided into two rooms by a movable wall which could be positioned at three different locations. The presence of an opening in this movable wall means that two rooms were considered: a transmitter room (TR) and a receptor room (RR). The configuration without the movable wall was also studied. Pressure profiles recorded with pressure gauges at ground level and on the wall presented numerous reflections. The damage effects were severe since the maximum overpressure never fell below 0.2 bar. Although this study is limited to a small scale and gaseous detonation charge, the results can be applied to a large scale and for a TNT charge.

Keywords: blast wave, confined explosion, explosion effects, overpressure, pressure profile, reflection, scaling

1. Introduction

Nowadays, safety in public, industrial, or military areas is a major concern. In spite of constant improvements in rules and standards, the risks linked to accidental or intentional explosions in industry are still significant. The numerous explosions reported demonstrate the importance of increasing the protection of people and structures in open, semi-confined, and full confined environments. Recent examples are the explosion in 2000 of a firework workshop (Enschede, the Netherlands) [1], in 2013 at the West Fertilizer Company (Texas, USA) [2], in 2015 a harbor warehouse (Tianjin, China) [3], and in 2016 the explosion in a manufacture of basic chemicals, fertilizers and nitrogen compounds, plastics, and synthetic rubber in primary forms (Coatzacoalcos, Mexico) [4]. A long list of terrorist attacks can be added to these industrial accidents. The most recent bombing attacks occurred on 13 May 2018, when a series of bombs exploded in three churches in Surabaya (Indonesia); on 1 July 2018, when a suicide bomber detonated a bomb in Jalalabad (Afghanistan); and on Easter Sunday 2019 when several bombs exploded in the capital of Sri Lanka, Colombo.

Numerous studies have been carried out in recent years to analyze the behavior of shock waves in the air [5–8]. While analytical, empirical, and numerical studies

have been conducted to predict the overpressure generated by the detonation of a solid or gaseous mixture in air, few studies have been done in closed environments, and most of the tools and models developed in air cannot be used in closed spaces because of the complex phenomenology of a confined detonation. Nevertheless, one can find in the literature several studies on semi-confined [9] or urban [10] configurations. Confined explosions present a serious safety hazard as significant damage to humans and structures is observed, unlike in free-field explosions.

Recent studies in a full confined environment are sparse, however, due to several limitations. In numerical studies the modeling of a full confined environment can become extremely costly in terms of computational resources. Researchers have therefore developed 1D/3D hybrid models to achieve a good balance between the accuracy of the results and the time required [11]. Experimentally, it is complex and costly to set up a full-scale experiment to study the propagation of the shock wave inside a building. As a result, studies on confined detonations are made at small scale. Reichenbach et al. [12] pointed out the interest of scaled experiments.

The advantages of small-scale experiments are their good flexibility and low cost. Thanks to the Hopkinson similarity law and the studies by Baker [13], the results recorded at small scale can be extrapolated to full scale if the charges are the same type between the two scales. Ohrt et al. [14] studied the propagation of a shock wave in a 1/12 small-scale model built from the full-scale model. The detonation of pressed TNT and a Composition A5 (98.5% RDX and 1.5% stearic acid) was studied and visualized in the small-scale model. A good correlation was found between the results at small scale and full scale.

Ram et al. [15] considered a single-story building at a 1:100 scale. Different configurations inside the building were investigated, all with an opening on the front face and inside. The shock wave was produced outside, impacted the front face, and propagated inside. The authors compared the internal geometry to a stiff porous building and depicted the pressure profile by a low-pass filter. They demonstrated that the simulation of full-scale experiments reproduced the scaled-up experiments.

The afterburning consequences on the shock wave reflection in confined spaces have also been investigated. The additional energy released by the secondary mechanism of combustion increases the energy in the whole flow field and increases the pressure. Therefore, the reflections interact with the post-combustion products. A quasi-static pressure is recorded in the case of a pyrotechnic explosive. Experimental and numerical studies have focused on the afterburning effect, for example, the work of Togashi et al. [16] and Milne et al. [17].

Hazard zones in confined rooms have been identified with a dual approach (experimental and numerical). Massoni et al. [18] investigated a three-level building at small scale and carried out numerical simulations. In this work the shock wave was generated by a shock tube placed in the vicinity of the model. Miura's team [19, 20] evaluated safety in nuclear fuel cycle facilities. The model comprised three rooms at ground level and two rooms on the second floor. Strong pressures were recorded on the corners and after diffraction around doors and windows. These studies showed that the corners of rooms are a critical zone.

Another relevant area of application for confined explosion studies is tunnels. For example, the experiments carried out by Binggeli et al. [21] and the simulations presented by Rigas et al. [22] and Benselama et al. [11] showed that the velocity and pressure of the blast wave are reinforced in long narrow geometries. The presence of an orthogonal pipe reduces the overpressure and is a good solution to ensure human safety.

In addition to their flexibility, small-scale experiments can reliably predict the behavior of shock waves in a confined area. When the building geometries are

complex, it is difficult to study and predict the behavior of the waves. Sauvan et al. [23] conducted an experimental characterization of the reflections coming from the detonation of a gaseous charge inside a cubic model. To obtain the most accurate characterization, the authors started with the free field and built the model wall by wall, making it possible to identify the first four reflected shocks.

The small-scale experiments conducted by Julien et al. [24, 25] on the behavior of shock waves coming from the detonation of a gaseous charge inside a small-scale warehouse led to the creation of predictive laws for the main characteristics of the shock wave. They also showed that critical zones exist in complex confined buildings.

Although confined explosions have been researched, the effects of the size of the opening between two rooms have not been fully established.

The present work concerns the volume and open area effect on the shock wave propagation inside a single-story building with an inner movable wall. The research is based on a small-scale experiment. The study focuses on the impact of the open area and of the room volume on the shock wave main pressure profiles and maximum overpressure.

This chapter describes the results obtained from these experiments. Pressure distribution is discussed and potential damage is highlighted.

2. Experimental setup

The experimental setup is a small-scale closed one-story building with a movable wall that can divide the building into two rooms: a transmitter room (TR) where the explosion (CE) takes place and a receptor room (RR). The walls are made of medium-density fiberboard (**Figure 1**). The internal dimensions of the building are length (L) 1.23 m, width (Lw) 0.51 m, and height (h) 0.24 m. All the walls have the same thickness e = 0.04 m. It means that the exterior dimensions are 1.31 m for the length, 0.59 m for the width, and 0.28 m for the height.
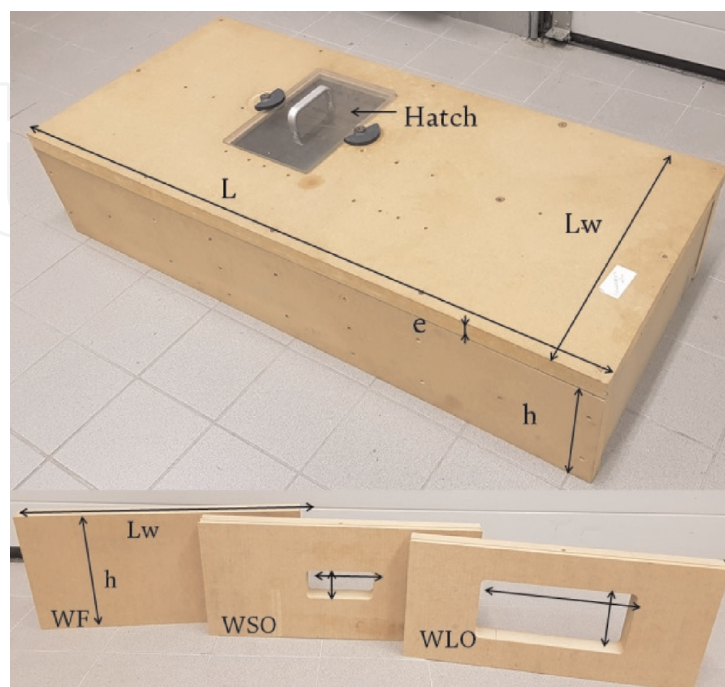

Figure 1.
Test facility.

The dimensions of the movable walls are Lw = 0.51 m and h = 0.24 m. Two types of movable wall were considered: a full wall (WF) and walls with an open area.

The openings are centered on the face. The wall with the smallest opening is denoted WSO, and the dimensions of its opening are 0.128 × 0.06 m, i.e., an area of 0.00768 m². The wall with the largest opening is denoted WLO, and the opening has an area of 0.0305 m² (0.254 × 0.12 m). The movable wall can be fixed at different locations inside the building to vary the volumes of the transmitter and receptor rooms.

Four configurations were examined (**Figure 2**). Configuration 1 is without the movable wall, configuration 2 has a movable wall located 0.275 m from the south wall, and configurations 3 and 4 have a movable wall located 0.594 m and 0.909
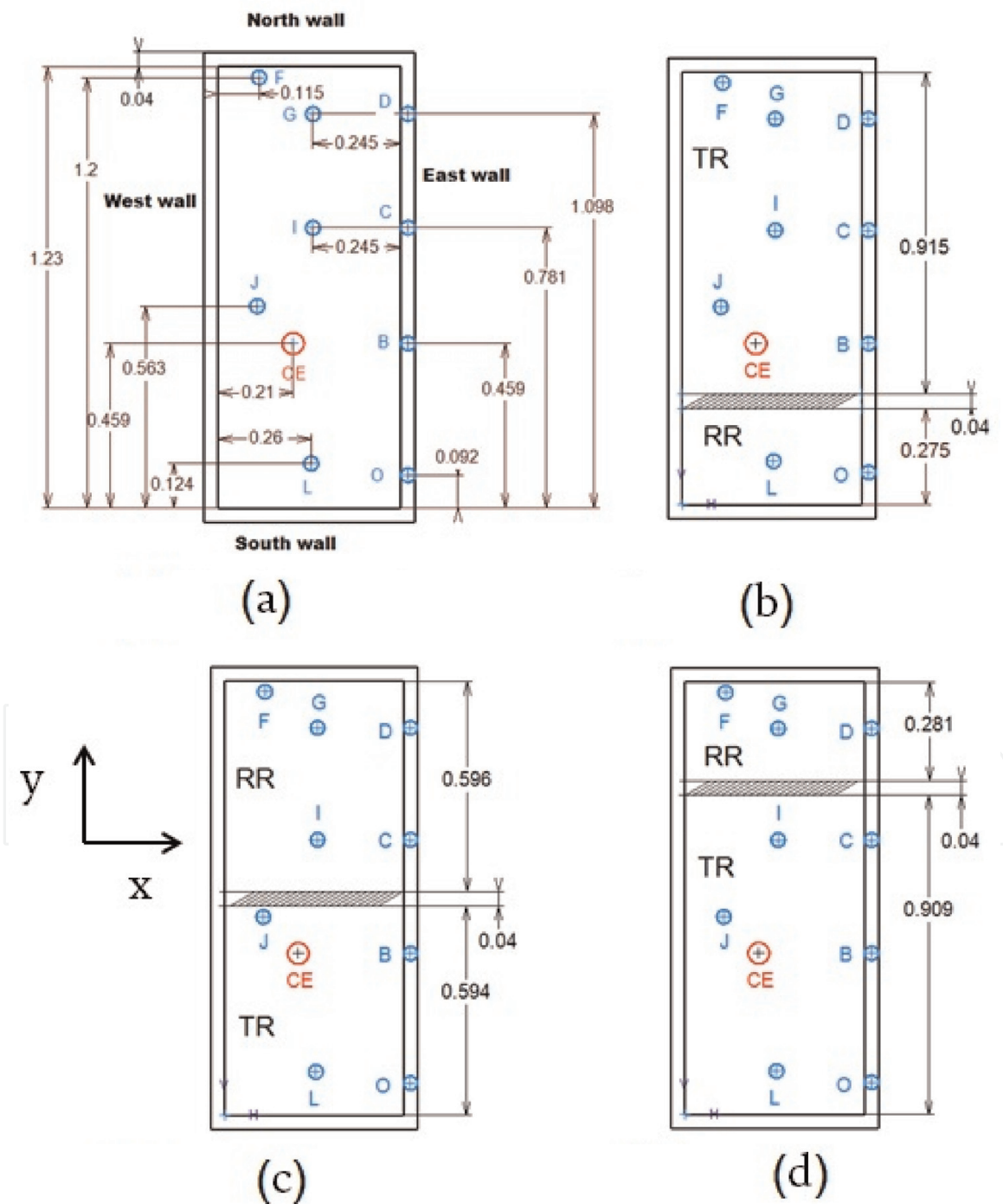

Figure 2.
Schematic experimental configurations with pressure gauges and explosive charge (CE) positioning:
(a) configuration 1, (b) configuration 2, (c) configuration 3, and (d) configuration 4.

from the south wall, respectively. In the text, we use the terms configurations 2, 3, and 4 or walls 2, 3, and 4.

The explosive charge is a stoichiometric propane oxygen ($C_3H_8 + 5O_2$) mixture confined in a hemispherical soap bubble with a radius of 0.07 m. The experiments were conducted at ambient temperature and pressure. The density of the gaseous mixture is 1.41 kg m^{-3}, so the mass of explosive charge is 1.0129×10^{-3} kg.

The detonation of the gaseous mixture is generated by an exploding wire fixed between two electrodes linked to a high-voltage supply. The exploding wire is transformed into a plasma and delivers severe conditions to initiate the detonation (all details can be found in [26]). The center of the explosive charge (CE) is fixed (**Figure 2**) for all the configurations studied. In C1 the distance between the south wall and the center of explosion is 0.459 and 0.771 m from the north wall. The distance between the movable wall and the center of explosion is 0.144 m in C2, 0.135 m in C3, and 0.450 m in C4. The volume of the transmitter room (TR) in C2 is $V_{TR-C2} = 0.1120$ m^3, in C3 is $V_{TR-C3} = 0.0727$ m^3, and in C4 is $V_{TR-C4} = 0.1113$ m^3. So, the volume of receptor room (RR) is $V_{RR-C2} = 0.0337$ m^3, in C3 is $V_{RR-C3} = 0.0729$ m^3, and in C4 is $V_{RR-C4} = 0.0344$ m^3.

Pressure histories were recorded over a 6 ms period with nine pressure transducers (Kistler 603B) at an acquisition frequency of 1 MHz. Five transducers (L, J, I, G, F) were distributed on the ground and four (O, B, C, D) on the east wall at half height (0.12 m). A layout of the sensor distribution with the different configurations (depending on the position of the movable wall) can be found in **Figure 2**. A sensor is considered protected when the shock wave cannot hit it directly.

3. Analytical approach to reflections

The pressure profile analysis requires knowing the type of reflection produced inside the single-story building. A preliminary study was carried out in order to identify whether there was a transition from regular reflection to Mach reflection and, if so, the height of the Mach stem. This transition between the two types of reflection is defined by a maximum angle β_{max} of oblique reflection which allows the formation of a Mach stem. For an incident shock at Mach 2.8, the limit angle β_{max} is 39.23°, and for a more intense incident shock, this angle reaches 39.97° [7].

The transition distance of formation R_{i0} is defined by [7]:

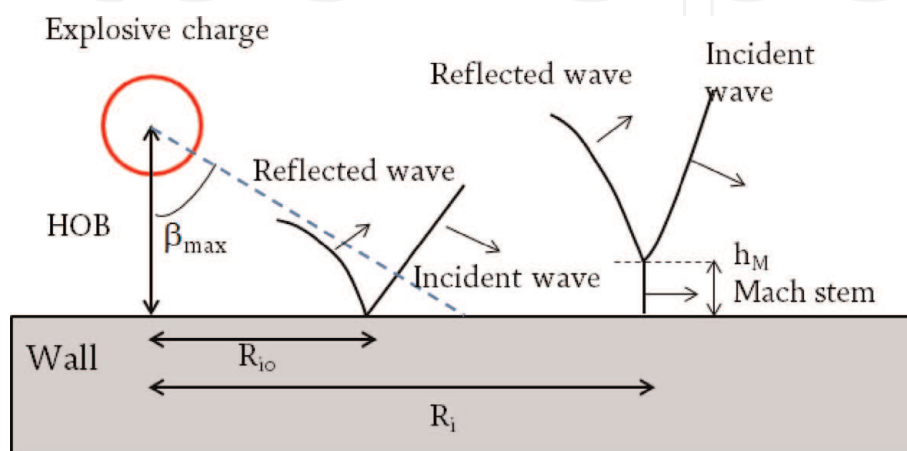$$R_{i0} = HOB. \tan{(\beta_{max})} \tag{1}$$

Figure 3.
Scheme of Mach stem formation.

and the height of the Mach stem h_M by:

$$h_M = 0.07 \, \text{HOB} \left(\frac{R_i}{R_{i0}} - 1 \right)^2 \tag{2}$$

where HOB represents the height of burst, i.e., the distance of the explosive charge center to the wall, and R_i is the distance from the wall (**Figure 3**).

On this basis, the distance R_{i0} and Mach stem height were calculated for each configuration by considering $\beta_{max} = 39.23°$. Only scenarios for which the Mach stem is received by a pressure gauge or by a wall are reported in **Table 1**.

Configuration	Wall reflection (WR)	R_{i0} (m)	Interest point	h_M at interest point (IP) (m)	Comments
1	East	0.245	L	3×10^{-3}	$h_M < d_{WR-IP}$
			I	2×10^{-3}	$h_M < d_{WR-IP}$
			G	0.054	$h_M < d_{WR-IP}$
	West	0.171	L	0.010	$h_M < d_{WR-IP}$
			I	0.010	$h_M < d_{WR-IP}$
			G	0.110	$h_M < d_{WR-IP}$
			F	0.160	$h_M > d_{WR-IP}$
2	East	0.245	I	2×10^{-3}	$h_M < d_{WR-IP}$
			G	0.054	$h_M < d_{WR-IP}$
			F	0.086	$h_M < d_{WR-IP}$
	West	0.171	I	0.011	$h_M < d_{WR-IP}$
			G	0.109	$h_M < d_{WR-IP}$
			F	0.162	$h_M > d_{WR-IP}$
	South	0.117	East wall	0.024	Impact on wall
			West wall	6×10^{-3}	Impact on wall
3	East	0.245	L	3×10^{-3}	$h_M < d_{WR-IP}$
			South wall	0.016	Impact on wall
	West	0.171	L	0.013	$h_M < d_{WR-IP}$
			South wall	0.041	Impact on wall
	North	0.110	East wall	0.028	Impact on wall
			West wall	8×10^{-3}	Impact on wall
4	East	0.245	L	3×10^{-3}	$h_M < d_{WR-IP}$
			I	2×10^{-3}	$h_M < d_{WR-IP}$
			South wall	0.016	Impact on wall
			North wall	0.015	Impact on wall
	West	0.171	L	0.013	$h_M < d_{WR-IP}$
			I	0.011	$h_M < d_{WR-IP}$
			South wall	0.041	Impact on wall
			North wall	0.039	Impact on wall

Table 1.
Location of Mach stem.

There can be no Mach reflection on the south and north walls in configuration 1, as the walls are not wide enough to reach a transition of reflection. The transition appears on the east and west walls. On the east wall, the transition is at y = 0.25 m (south-north) from the CE. The height of the Mach stem is <1 cm at y = 0.322 m and reaches 0.05 m for y = y_G = 0.639 m. These heights are lower than the distance of the east wall to gauges I and G. However, the study of the reflection on the west wall leads to a transition distance of 0.17 m and a Mach stem height of 0.01 m for y = y_I = 0.322 m, 0.1 m for y = y_G = 0.639 m, and 0.16 m for y = y_F = 0.741 m. This implies that only gauge F is impacted by the Mach reflection.

In most cases, the results of the calculations reported in **Table 1** show that the height of the Mach stem does not exceed 0.1 m. Only gauge F can be impacted by the Mach stem in configurations 1 and 2 after reflection on the west wall. **Table 1** highlights that if a reflection is produced on a wall with a transition, then the Mach stem can reach a lateral wall. This is the case, for example, in configuration 3 with the reflection of the west wall. The Mach stem arrives on the south wall with a height of 0.04 m and a height of 0.028 on the east wall. This is also the case for configuration 4 if we consider the reflection on the west wall: the Mach stem impacts the south and north walls with a height of 0.04 m.

4. Pressure profile analysis

4.1 Effect of opening size on pressure profiles

The pressure profiles recorded in a confined building are complex due to the multiple reflections. In this part, the pressure signals are analyzed by considering the free field and C1 and the presence of the movable wall in C3 without and with an opening.

4.1.1 Gauges on the ground

4.1.1.1 Gauge J

In free field (**Figure 4a**), the secondary shock is detached from the incident peak at 0.297 ms with ΔP^+ = 0.098 bar. This secondary shock is amplified by the confinement and reaches 0.264 bar. After detonation of the explosive charge, a first shock wave propagates into the surrounding air, and a rarefaction wave propagates toward the center of charge. Once the rarefaction wave decreases the inside pressure, a new shock appears and propagates to the origin and reflects [27]. The effect of confinement in configuration 1 produces small reflection waves and consequently a small overpressure. The overpressure is limited to 0.2 bar with a peak at 0.5 bar.

The mobile wall P3 creates several reflections (**Figure 4b**) which are represented by the pressure peaks. Wall 3 is only 0.031 m away, so the second peak arrives immediately after the incident shock. The overpressure is increased to 3.6 bar due to the direct reflection.

The most severe peak appears later at 2 ms and reaches 4.7 bar. This peak decreases and arrives later with the presence of an opening in wall 3. The energy of the incident shock is not confined in the transmitter room but is partially transmitted to the receptor room. The smaller peak at 0.55 ms is stronger with the larger opening. This can be explained by the diffraction of the shock on the corner of the opening in the direction of gauge J. The corner of the larger opening is closer to gauge J than that of the smaller opening.
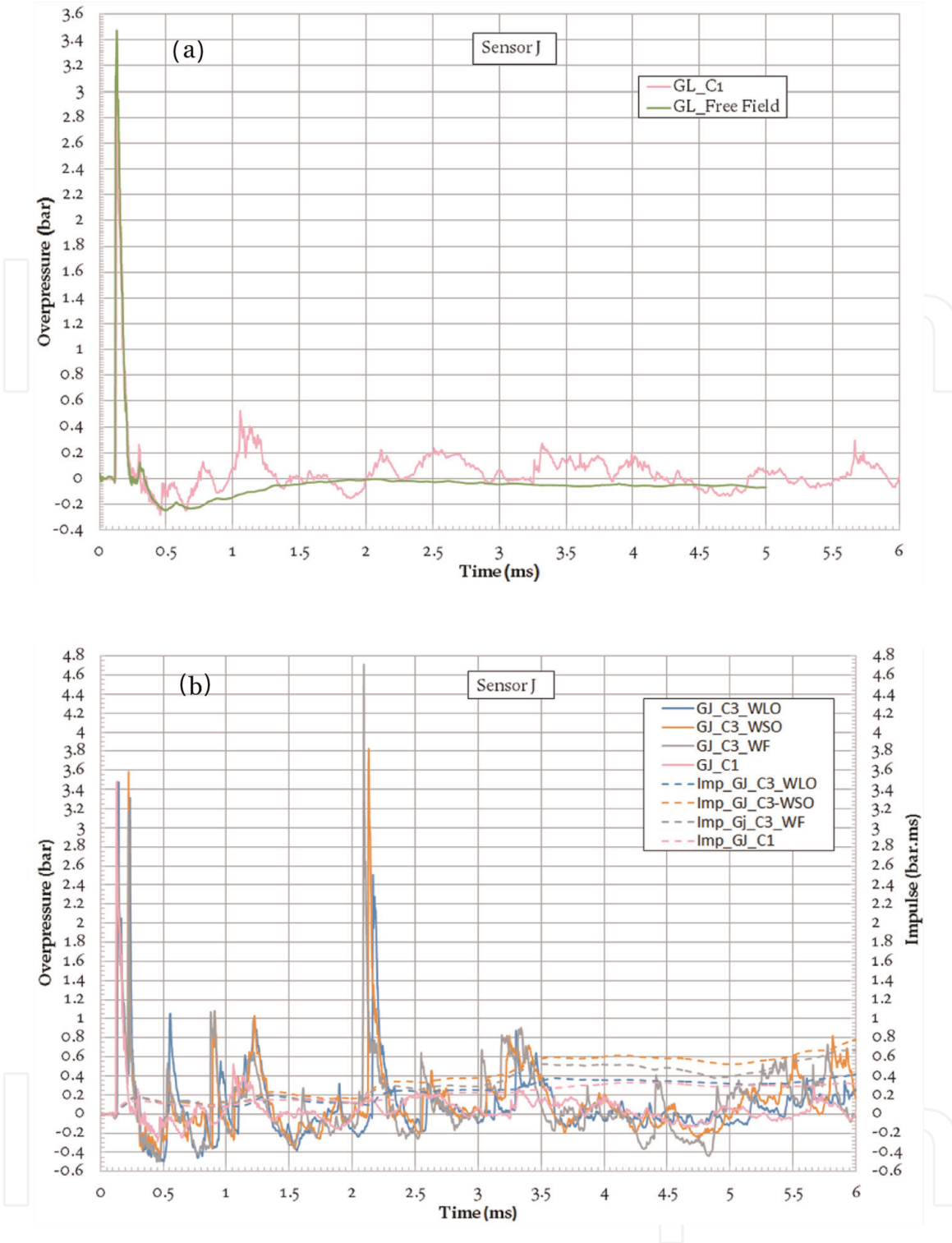
Figure 4.
Pressure and impulse histories. Gauge J: (a) comparison of free field and C1 and (b) configurations 1 and 3.

4.1.1.2 Gauge L

In the single confinement (C1), gauge L is closer to the south wall (0.124 m). In this infoduration, the second peak is the maximum overpressure (**Figure 5a**) and comes from the south wall with a reflection coefficient on the order of 2. This is verified by applying the classical normal reflection equation [7]:

$$\frac{P_r}{P_i} = \frac{(3\gamma - 1)\frac{P_i}{P_0} - (\gamma - 1)}{(\gamma + 1) + (\gamma - 1)\frac{P_i}{P_0}} \tag{3}$$

where P_r and P_i are the absolute reflected and incident pressure and P_0 is the ambient pressure. In this case $P_i = \Delta P_i + P_0 = 1.794$ bar.

After that, the reflected shock interacts with the reflected wave from the west wall and the east wall. Strong negative pressures (-0.35 bar) are observed during an expanded time (1–5 ms) and provide an average impulse around 0.3 bar ms which reaches the value 0.44 ms.

The peak at 2.6 ms is not induced by the north wall because it is present in configuration 3 (**Figure 5b**). Wall 3 leads to new peaks at 2 and 4 ms. They correspond to a decreasing phase for configuration 1. They can emerge from the
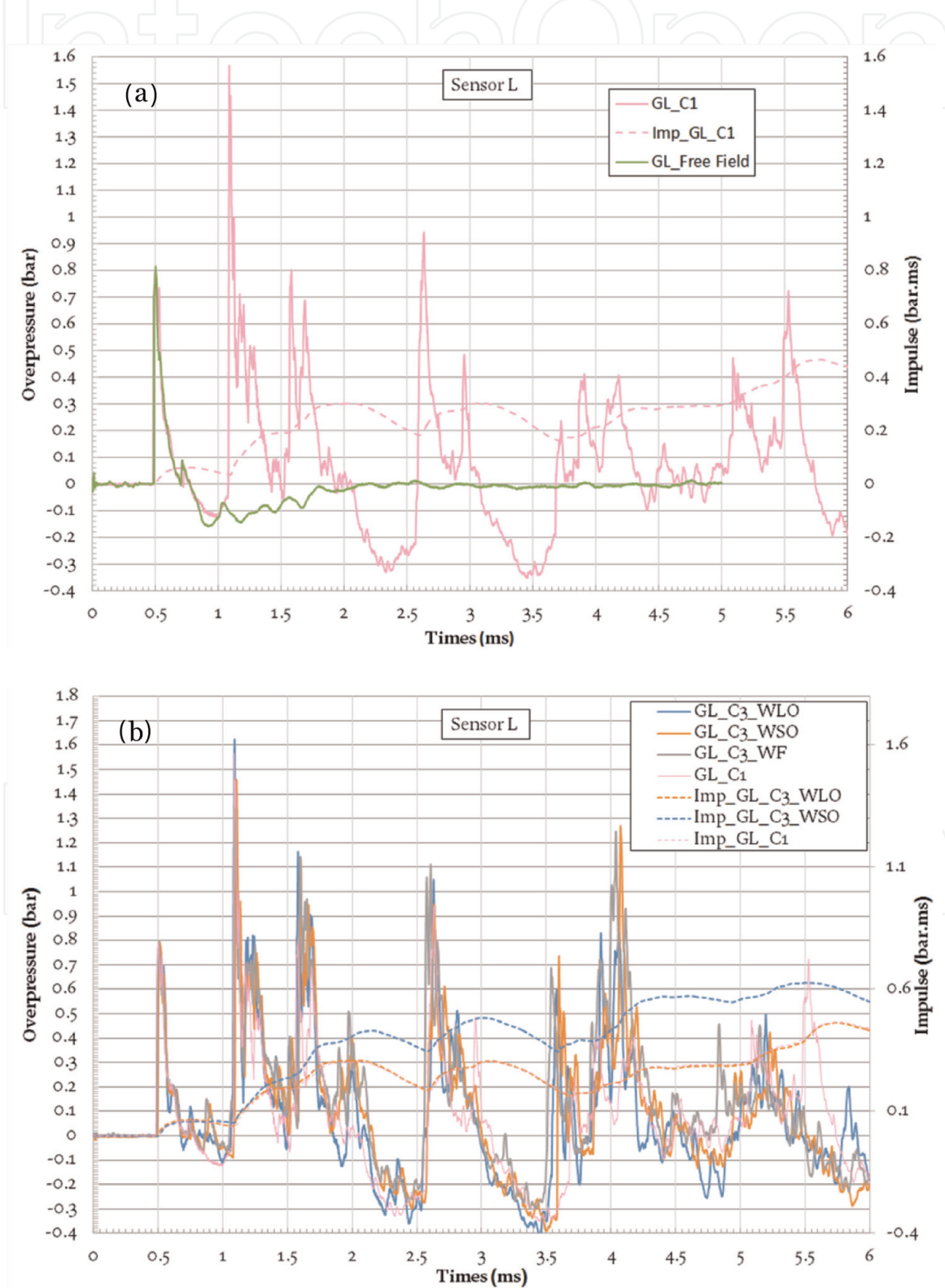

Figure 5.
Pressure and impulse histories. Gauge L: (a) comparison of free field and C1 and (b) configurations 1 and 3.

presence of a small Mach stem on the south wall coming from reflection on the west wall and another small Mach stem on the east wall coming from the north wall (**Table 1**). The pressure profiles versus the size of opening are very similar with a decrease in the overpressure with the increase in event size. A time offset appears after 3 ms with the presence of wall 3. A negative phase appears at 1.9 ms for the large opening and at 4.8 ms with the two openings. This is due to diffraction at the angles of the vent and consequently the generation of rarefaction waves. These rarefaction waves catch up the reflected waves and decrease them, as observed by Rose [28]. This phenomenon increases the impulse with the opening.

4.1.1.3 Gauge I

A strong overpressure is recorded at the same time (1.09 ms) and with an amplitude similar to the pressure profile from gauge L (**Figure 6a**). The overpressure is 1.595 bar for gauge I and 1.578 bar for gauge L. The peak cannot be explained by a unique reflection on the nearest wall (east wall) but by the cumulative effect of the reflected waves from the west and east walls. The reflection by the ceiling can be found at 1.25 ms.

After a negative phase, an increase in pressure up to 1.2 bar at 2.6 ms is observed and comparable to the peak recorded on gauge L. Three wave trains can be distinguished, corresponding to three time ranges: (1) 1.38–1.77 ms, (2) 3.5–4.12 ms, and (3) 4.8–5.56 ms.

Wall 3 (**Figure 6b**) mitigates the level of overpressure with a delay that increases when the size of the opening decreases. The larger opening decreases the overpressure at 2 ms from 4.7 bar to 2.54 bar (ratio of 1.85) with a time delay of 0.055 ms. Of course, the full wall 3 totally obstructs the propagation of the shock wave in the receptor room. The impulses are comparable in terms of evolution and magnitude between configuration 1 and configuration 3 with the larger opening.

4.1.1.4 Gauge G

Gauge G is located near the north wall. **Figure 7a** shows several peaks with an amplitude higher than 0.3 bar in the range of 6 ms. The ratio of the maximum overpressure between the first reflected wave and the incident wave is on the order of 2. However, on gauge G, the second peak is not the maximum overpressure reached. The maximum appears at 3.9 ms and is equal to 0.787 bar.

The negative phase is lower than that observed on gauge I. The wave train identified on gauge I can be recognized on gauge G. The wave train is more extended in time and amplified compared to the first reflection and the peak at 2.6 ms on gauge I.

As expected, the greater the obstruction by wall 3, the later the wave arrives in the receptor room and the more the overpressure decreases (**Figure 7b**). The negative phases resulting in configuration 1 disappear with the presence of wall 3 and correspond to a positive phase. Nevertheless, negative phases are still observed in the case of wall 3 with the smaller opening. The impulses increase linearly and are higher on this gauge than on gauge I: 0.4–0.5 bar ms against 0.35 bar ms for gauge I.

4.1.1.5 Gauge F

Gauge F is the closest gauge to the north wall. A wave train arrives almost simultaneously with the incident shock wave (**Figure 8a**).

The three wave trains identified on gauges I and G are still present on gauge F. On gauge F, there is an amplification of the overpressure during the first wave train
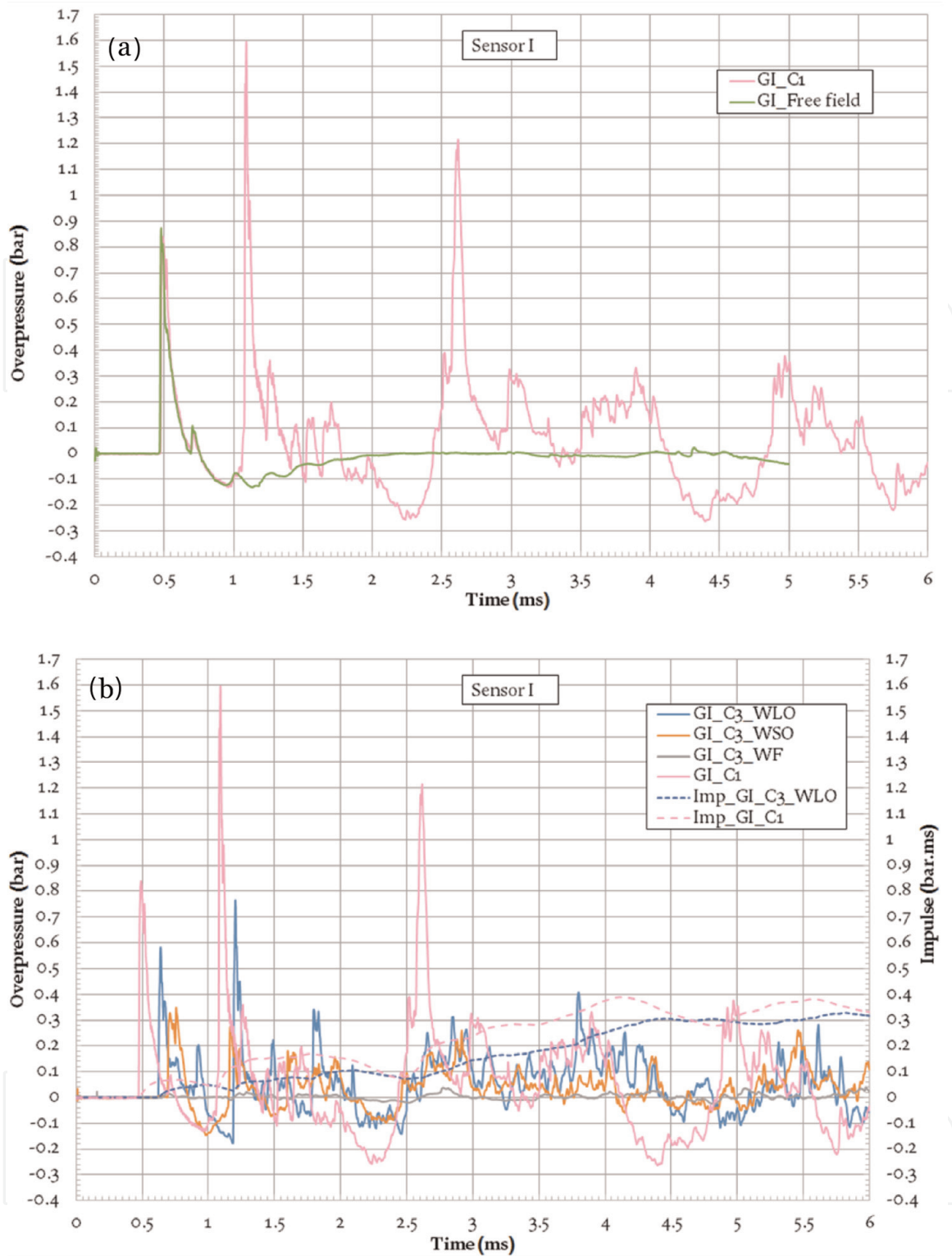
Figure 6.
Pressure and impulse histories. Gauge I: (a) comparison of free field and C1 and (b) configurations 1 and 3.

(1.54–2.6 ms), whereas the last one is mitigated compared to gauge G. This amplification can be explained by the presence of a Mach reflection identified previously (**Table 1**). The aggregation of the waves represents the interaction of the reflected waves coming from reflection on the four walls and the ceiling.

With wall 3 (**Figure 8b**), there is no negative phase. All the overpressures are strongly mitigated with the reduction in the opening size and totally mitigated with the full wall 3. However, a global view of the pressure profile shows that the same peaks can be identified without or with wall 3 with opening. This means that the reflected waves are produced in the second part of the building, i.e., in the receptor
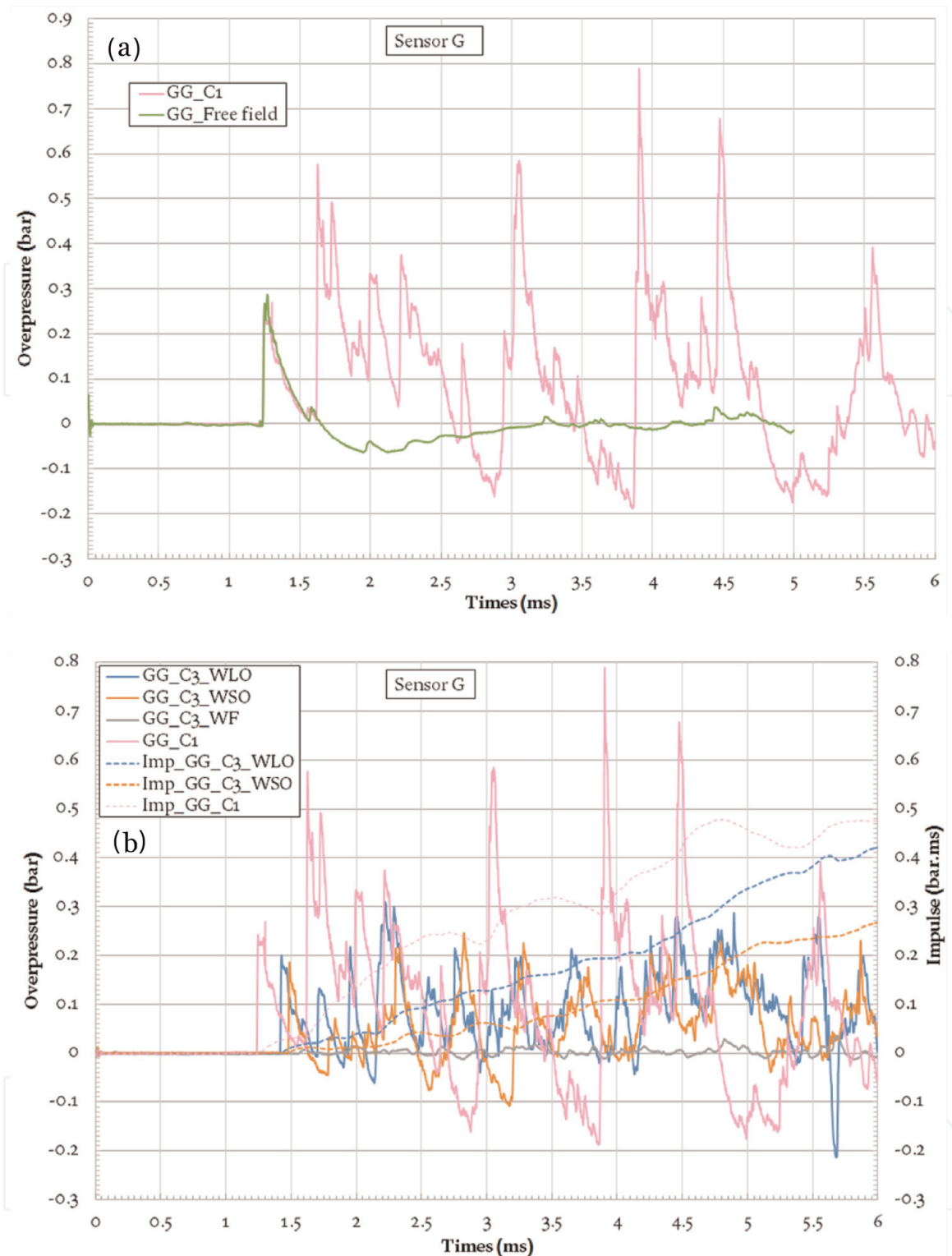
Figure 7.
Pressure and impulse histories. Gauge G: (a) comparison of free field and C1 and (b) configurations 1 and 3.

part. The impulses obtained on gauge F are similar to those recorded on gauge G in terms of evolution and magnitude.

4.1.2 Gauges on the east wall

Gauge B is directly impacted by the explosion (**Figure 9a**). This gauge undergoes the most severe overpressure (2.4 bar) but the lowest impulse compared to the other gauges. Negative phases recorded on gauge B correspond to positive
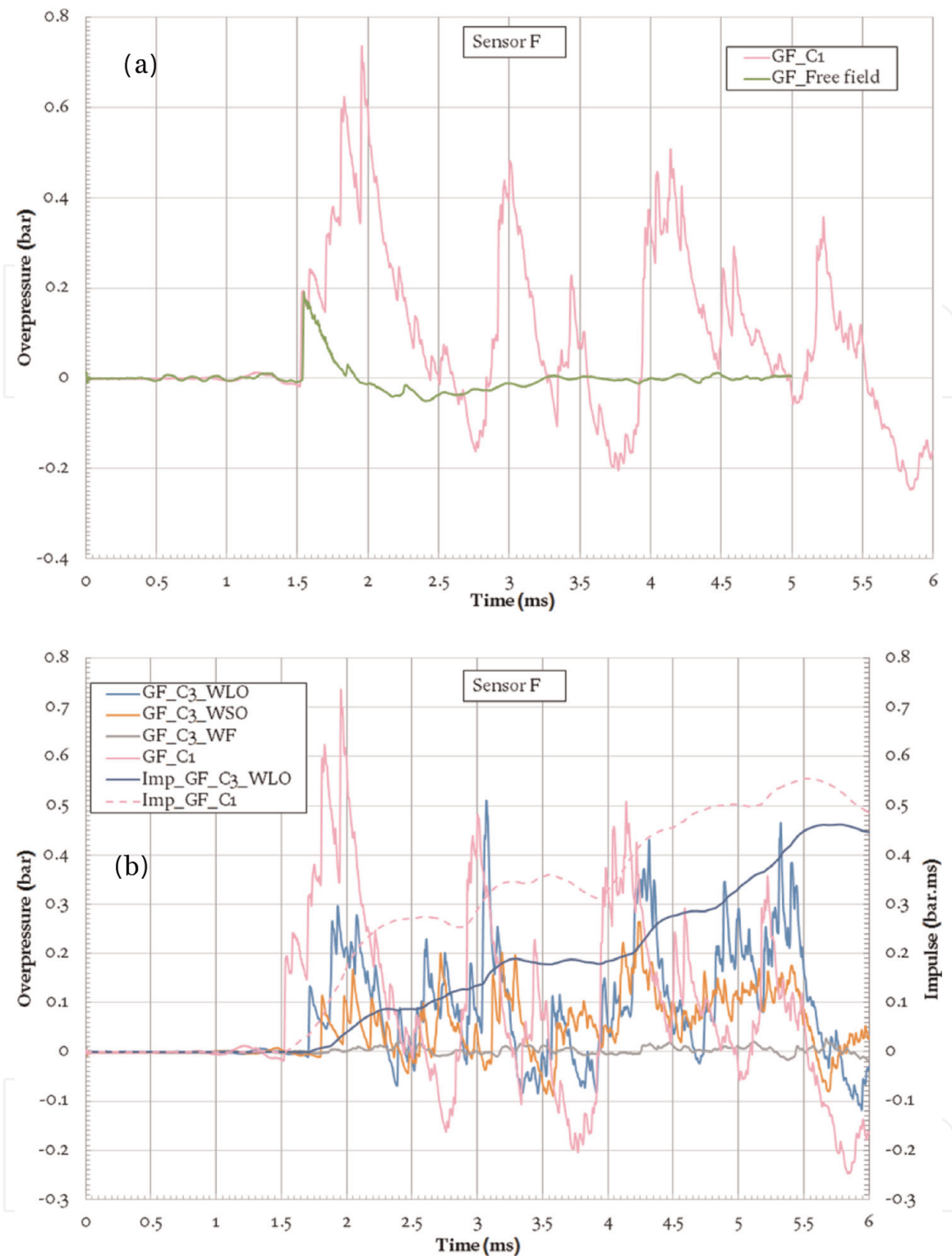
Figure 8.
Pressure and impulse histories. Gauge F: (a) comparison of free field and C1 and (b) configurations 1 and 3.

phases on gauge O (**Figure 9b**) and vice versa. The time delay of arrival on gauge O is not enough to explain the alternating phases.

The first two peaks until 1.3 ms observed on gauges C (**Figure 9c**) and O are superimposed. This is due to the almost identical distances of gauges O and C from the center of the explosive charge (0.489 and 0.456 m, respectively). Strong overpressure appears (0.9 bar, 1.5 ms) on gauge O due to the proximity of the south wall. On gauge C, a wave train with an overpressure above 0.3 bar is maintained between 2.8 and 3.7 ms, leading to a higher impulse level.

Gauge D receives the first wave later (1.4 ms), and the maximum of overpressure (1.2 bar) is reached at 3.5 ms (**Figure 9d**).
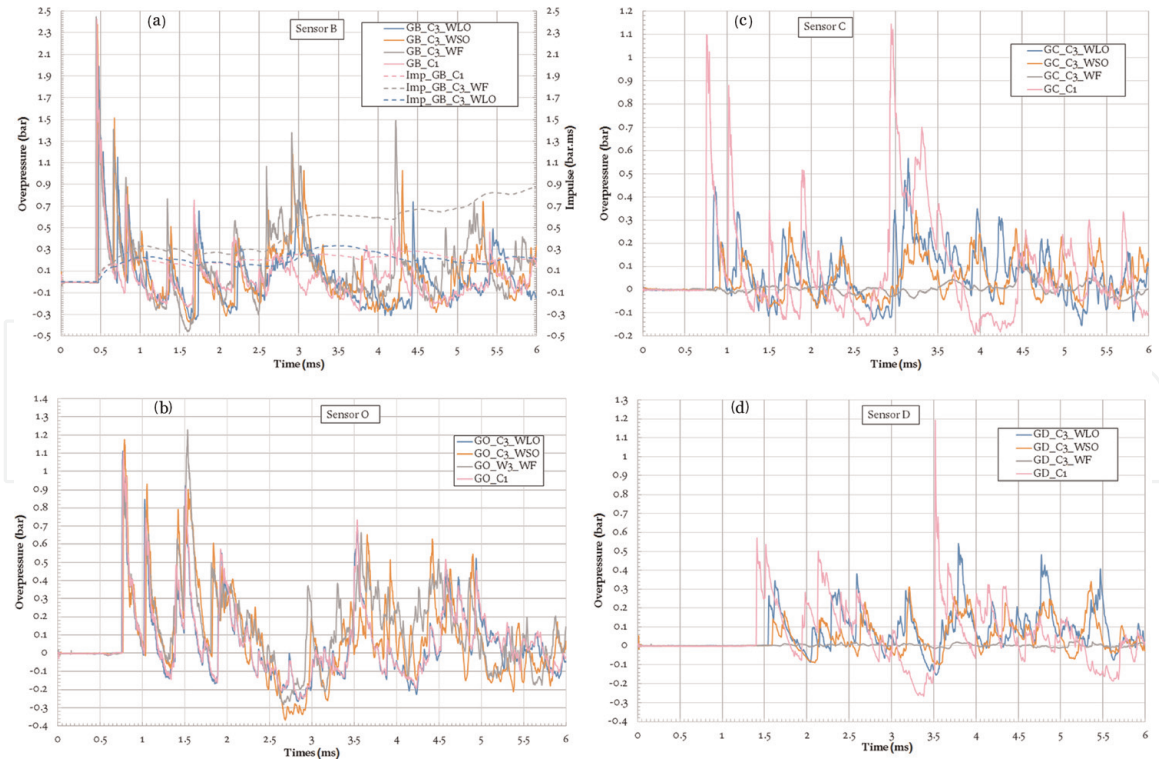
Figure 9.
Pressure and impulse histories. Configurations 1 and 3: (a) gauge B; (b) gauge O; (c) gauge C and (d) gauge D.

A similar evolution of pressure profiles is obtained on gauges I (**Figure 6b**) and C (**Figure 9c**) even if the waves arrive early. The same behavior is noted between gauges G and D (**Figure 7b** and **d**).

Wall 3 has little effect on the pressure profile of gauge O, except for a new peak with an overpressure of 0.37 bar at 2.95 ms. The overpressure decreases as the size of the opening increases. On gauges C and D, the overpressure increases with the size of the opening of the movable wall in configuration 3.

4.2 Effect of location of the movable wall on pressure profiles

In this section, the analysis concerns the effect of the volume in the transmitter room, i.e., the position of the movable wall inside the building. Here, we focus on gauges J and F and configurations with a full wall and with the larger opening of the wall.

4.2.1 Gauge J

In each configuration, gauge J is in the transmitter zone (**Figure 2**). Unfortunately, it is only possible to check the incident overpressure of the shock wave in configuration 4 due to a thermal drift (**Figure 10a**). However, the pressure profiles obtained in configurations 1 and 2 with the full wall are similar and different from configuration 3 examined in the previous section.

The presence of an opening in the mobile wall (**Figure 10b**) does not affect the response of gauge J in configurations 1, 2, and 4.

4.2.2 Gauge F

Gauge F is located near the north wall. So, this gauge is totally protected in configurations 3 and 4 with a full movable wall.
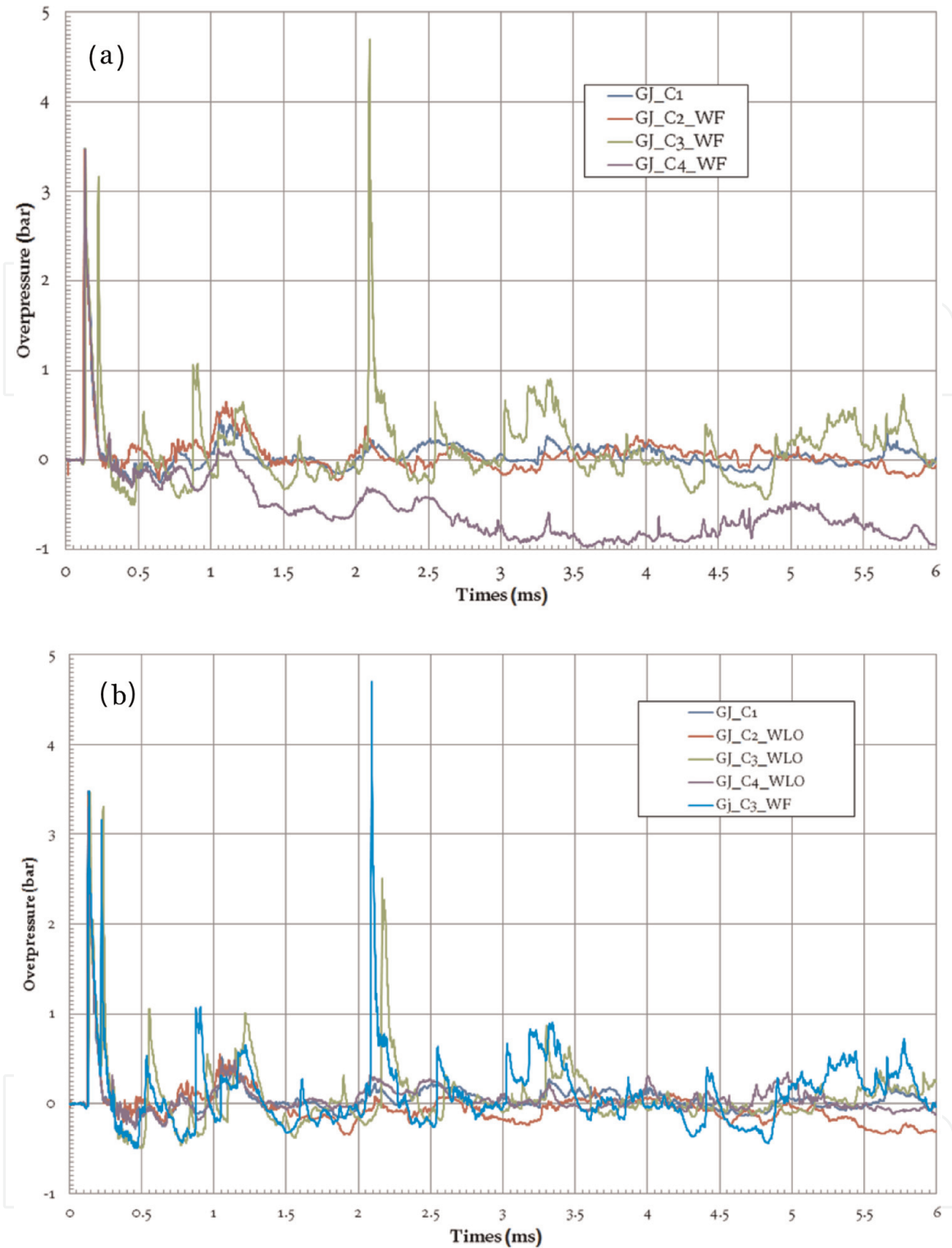
Figure 10.
Pressure histories. Gauge J, configurations 1–4: (a) with full wall and (b) with large opening for C2, C3, and C4.

The effect of the location of the movable wall is only perceptible above 2.2 ms. The wall deletes the negative phase existing before 3 ms in configuration 1 (**Figure 11a**). So, the overpressure is high in configuration 2. However, a series of three negative phases is recorded between 3.5 and 5.2 ms.

In the case of configurations with an opening in the mobile wall (**Figure 11b**), gauge F is not protected. The opening in configuration 2 mitigates all the pressure by filtering the peaks at 3.3 ms and 3.94 ms. In configurations 3 and 4, the negative phase is almost nonexistent. The more the volume of the receptor zone decreases, the more the overpressure signals are absorbed, falling to below 0.3 bar in configuration 4.
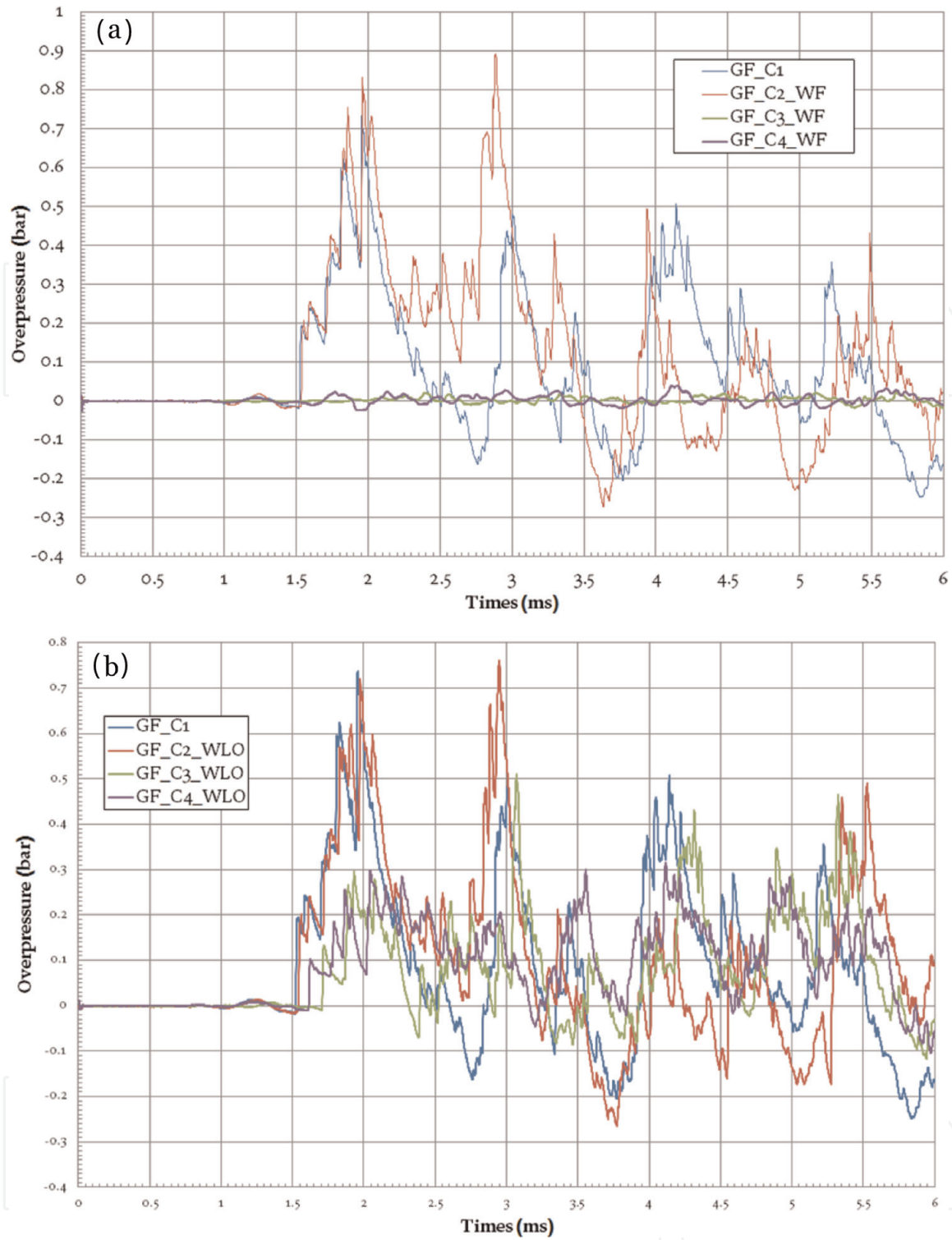
Figure 11.
Pressure histories. Gauge F configurations 1–4: (a) with full wall and (b) with large opening for C2, C3, and C4.

5. Mitigations and effect zones

Here we analyze the global pressure field and its effects inside the building. The data are expressed as a function of the scaled distance Z (m kg$^{-1/3}$) which is defined as $Z = R.M^{-1/3}$ where R is the radial distance from the charge center and M is the mass of the gaseous mixture. The evolution of overpressure in free field is represented by the following law [26]:

$$\text{Ln}\frac{\Delta P}{P_0} = 1.98458 - 1.93917 \ \text{ln} \, Z + 0.100553 \, (\text{ln} \, Z)^2 \ \text{with } 0.8 \leq Z\left(\text{m kg}^{-1/3}\right) \leq 53.4 \quad (4)$$

For confined geometries, the shortest path leading from the charge to the gauge position can be predicted by studying the reflections and diffractions encountered by the shock wave to reach the studied interest point (**Figure 12**).

Using this path, as illustrated in **Figure 12**, a set of confined scaled distances Z_{conf} is calculated by the following methodology. The shortest path gives a new set of radial distances between the center of the explosion and the sensor (R_{conf}). The distance R_{conf} is correlated with the cubic root of the mass of gaseous mixture (M). Hence, the confined scaled distance is calculated by $Z_{conf} = R_{conf}.M^{-1/3}$.

To compare the overpressure measured in a confined environment with the corresponding one in free field at the same distance, the scaled distance Z_{conf} is used in Eq. (4).

5.1 Ground level

At ground level, for all the configurations with no opening (**Figure 13a**), the overpressure is always higher than the overpressure in free field (without confinement). Examination of the case with no opening means that the transmitter room is of course the only room studied. No amplification is obtained on gauge J in configurations 1, 2, and 4. The effect of the mobile wall close to gauge J in configuration 3 leads to a stronger overpressure. Configuration 2 leads to a ratio of 4 at position F, which is higher than the corresponding ratio in configuration 1. For gauges I and L, the ratio varies on average between 1.3 and 2.0.

The presence of an opening in the mobile wall means that two rooms need to be considered: a transmitter room and a receptor room (**Figure 13**).

In the receptor room, the small opening efficiently decreases the overpressure. A ratio of $\Delta P/\Delta P_{FF}$ below unity is reached on gauges I and L for configurations 2 and 3 and near 1 on gauge G for configuration 3. For configuration C4, the maximum overpressure is higher than the corresponding free field. Gauge G is directly exposed to the propagation of the shock wave, whereas gauge F is located at the limit of direct view. Hence, the overpressure on gauge G is higher than for gauge F. The mitigation decreases with the opening size. So, for gauge L the ratio varies from 0.55 to 0.7 for the small and large opening. The other positions in the receptor room show an overpressure higher than in free field, particularly on gauge G: the ratio on gauge G is 1.16 in C3 and 3.7 in C4.

In the transmitter room and configuration 2, the overpressure decreases on gauge F with the increase in the opening size. The large opening reduces the maximum overpressure on gauge G and the overpressure remains unchanged with the small opening compared to the same configuration with the full wall. The larger opening generates an increase in the overpressure on gauge L in configurations 4 and 3 and on gauge I in configuration 2.
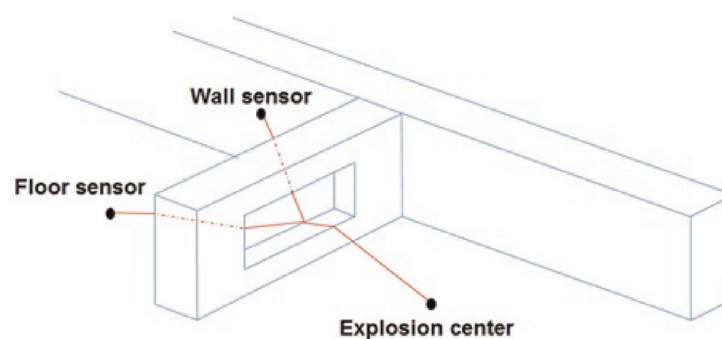
Figure 12.
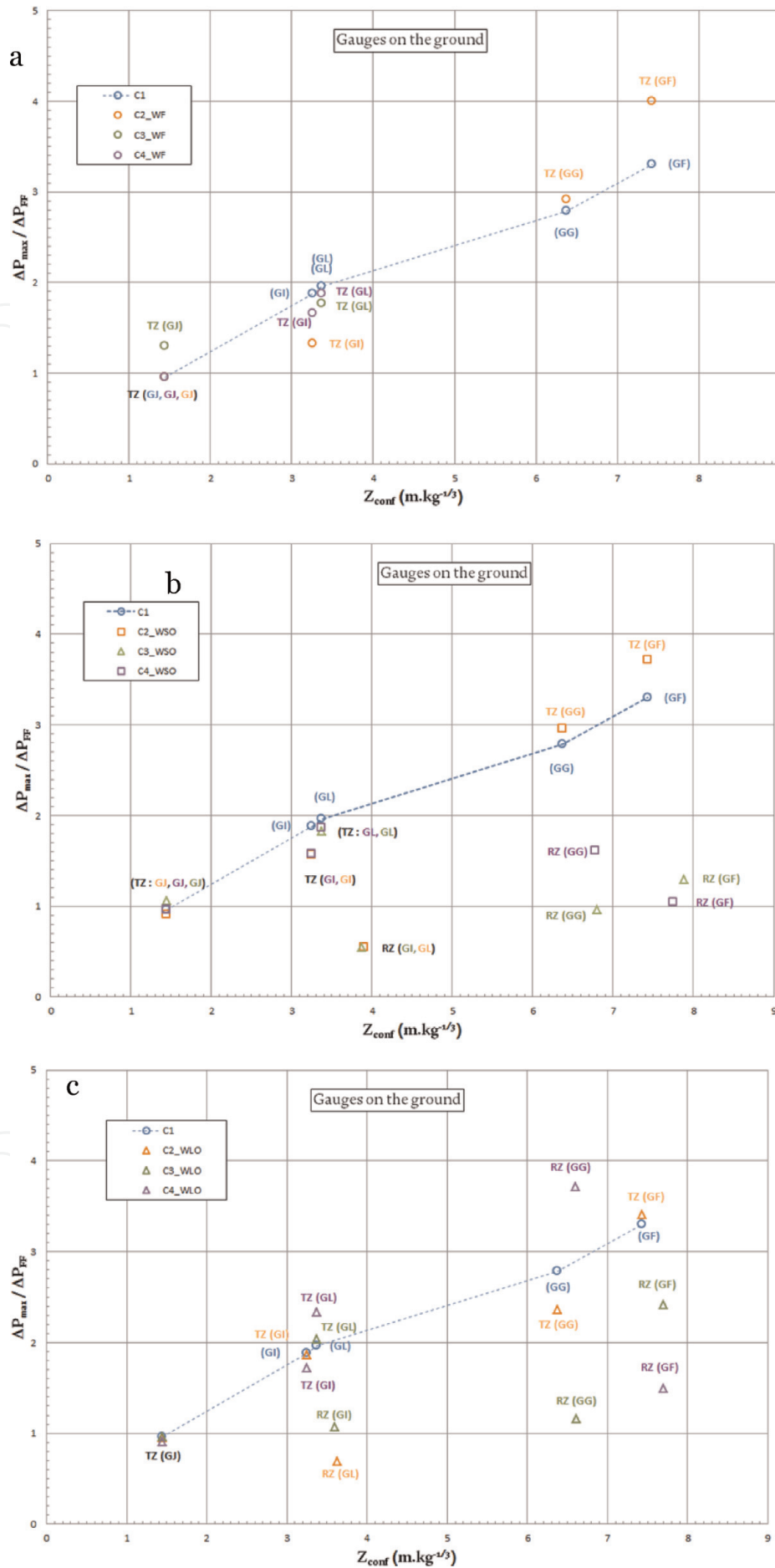*Example of shorter path through the opening.*

Figure 13.
Ratio of the maximum overpressure at ground level to the overpressure in free field versus the scaled distance in confined room. Pressure histories: (a) with full wall; (b) with small opening for C2, C3, and C4; and (c) with large opening for C2, C3, and C4.

5.2 On the walls

The overpressures were measured on the east wall with gauges located at half height of the wall. As expected, the overpressures are higher on the wall than on the ground. With the full wall (**Figure 14a**), gauge D is in the unprotected zone for configurations 1 and 2.

The ratio $\Delta P/\Delta P_{FF}$ is in the range 2 and 3 for all the other gauges and configurations. This level is higher than the overpressure level recorded on the ground for the same configurations and for a reduced distance $Z \leq 7\,\mathrm{m}\ \mathrm{kg}^{-1/3}$. Considering the smaller opening (**Figure 14b**), the gauges in the receptor room are protected, and the ratio of overpressure does not exceed 1.6 bar.

For gauges C and O, the ratio is lower than unity, which is consistent with the measurement recorded on the ground for the same configurations with, respectively, gauges I and L. The large opening (**Figure 14c**) does not mitigate the overpressure lower than in the free field, but it decreases the overpressure at location D with respect to configuration 1. Consequently, on the wall, the overpressure ratios are in the same order as on the ground. The large opening is efficient and limits the ratio to 3 with respect to the free field. Gauge D presents a dangerous location for configuration 1 as it is obtained with gauge F on the ground.

5.3 Effect zones on the ground

As defined in the French pyrotechnic legislation and the ministerial order No. DEVP0753277A on 20 April 2007 and DEVP0540371A on 29 September 2005 and the applicable version on 6 May 2019 [29], all explosives may result in five effect zones classified according to the damage caused to persons and property (**Table 2**).

Table 3 gives all the maximum overpressures obtained for all configurations and all gauges.

The table clearly highlights that the pressure field is mainly higher than 0.43 bar, which means that damage zone Z1 is dominant. Cases with $\Delta P_{max} < 0.43$ bar are indicated in green and correspond to the receptor zone with small opening in the mobile wall except for three cases in configuration 3 (gauge G) and configuration 4 (gauges F and D). Outside the zones isolated by a full movable wall, the maximum overpressure is never below 0.2 bar. This means that in these domains the damage zone is classified in Z2.

5.4 Applications to TNT charges and scale-up to large scale

The investigation proposed here can be applied to a TNT charge. The comparison of the pressure effect between the gaseous mixture ($C_3H_8 + 5O_2$) and the TNT charge is shown in **Figure 15**. The evolution for the TNT charge was extracted from the Unified Facilities Criteria [30]. In **Figure 15**, the incident experimental overpressure at ground level (gauges L, J, I, and G) is reported.

The comparison between the two explosive charges is expressed by the TNT equivalency, as detailed in [26]. This pressure-based concept is only considered for the object of this investigation. The equivalent mass of an explosive pressure is given by the mass ratio of TNT (M_{TNT}) to the considered explosive (M) that produces the same peak overpressure at the same radial distance of each load, hence:

$$E_{P\text{-}TNT} = \frac{M_{TNT}}{M} = \left(\frac{Z}{Z_{TNT}}\right)^3 \qquad (5)$$
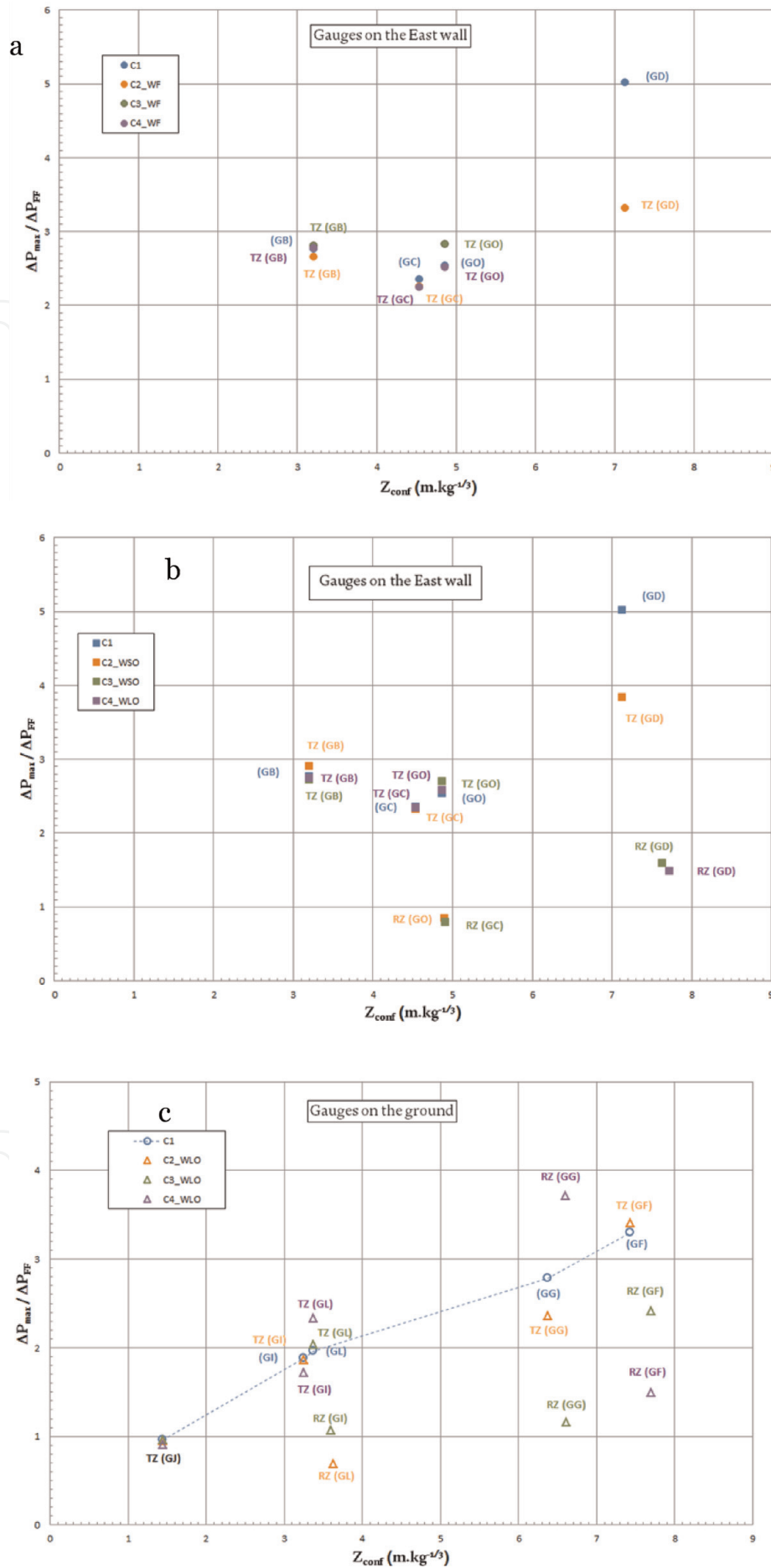
where Z is the scaled distance.

Figure 14.
Ratio of the maximum overpressure on the walls to the overpressure in free field versus the scaled distance in confined room. Pressure histories: (a) with full wall; (b) with small opening for C2, C3, and C4; and (c) with large opening for C2, C3, and C4.

Zone designation	Overpressure (bar)	Human casualties	Property damage
Z1	$\Delta P_{max} \geq 0.43$	Extreme (death 50%)	Extreme
Z2	$0.43 < \Delta P_{max} \leq 0.20$	Very serious	High domino effect
Z3	$0.20 < \Delta P_{max} \leq 0.14$	Serious	Serious
Z4	$0.20 < \Delta P_{max} \leq 0.14$	Significant	Light
Z5	$0.20 < \Delta P_{max} \leq 0.14$	Indirect injuries by breaking glass	Destruction of window

Table 2.
Effect zones for overpressure [29].

ΔP_{max} (bar)	C1	C2	C2-WSO	C2-WLO	C3	C3-WSO	C3-WLO	C4	C4-WSO	C4-WLO
Gauge L	1.6	/	**0.3 r**	0.5 r	1.4	1.5 t	1.6 t	1.5	1.5 t	1.9 t
Gauge J	3.5	3.5	3.3 t	3.4 t	4.7	3.8 t	2.5 t	3.5	3.5 t	3.3 t
Gauge I	1.6	1.1	1.3 t	1.6 t	/	**0.4 r**	0.8 r	1.4	1.3 t	1.5 t
Gauge G	0.8	0.8	0.8 t	0.7 t	/	**0.2 r**	**0.3 r**	/	**0.4 r**	1 r
Gauge F	0.7	0.8	0.8 t	0.8 t	/	**0.3 r**	0.5 r	/	**0.2 r**	**0.3 r**
Gauge O	1.1	/	**0.4 r**	0.6 r	1.2	1.2 t	1.1 t	1.1	1.1 t	1.1 t
Gauge B	2.4	2.3	2.5 t	2.3 t	2.4	2.4 t	2.0 t	2.4	2.4 t	2.4 t
Gauge C	1.1	1.1	1.1 t	1.1 t	/	0.4 r	0.6 r	1.1	1.1 t	1.1 t
Gauge D	1.2	0.8	0.9 t	0.7 t	/	**0.4 r**	0.5 r	/	**0.4 r**	**0.4 r**

Notations: r, receptor zone; t, transmitter zone; /, isolated zone; in bold, $\Delta P_{max} < 0.43$ bar.

Table 3.
Maximum overpressure in bar for all configurations.
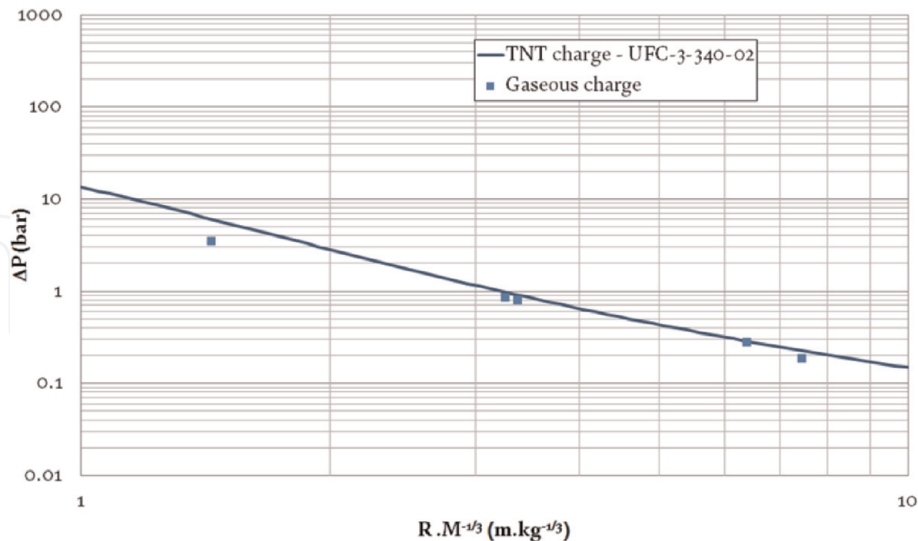

Figure 15.
Comparison of overpressure versus scaled distance for TNT and gaseous charge.

A TNT mass in the range of 0.49–0.96 g is deduced by applying Eq. (5).

The comparison of reflected overpressure was performed on the basis of abacus reporting in UFC-3-340-02 [30] and converted here into SI units (**Figure 16**).

For each gauge on the wall, the incident overpressure ΔP_i corresponding to the scaled radial distance is calculated from Eq. (4).
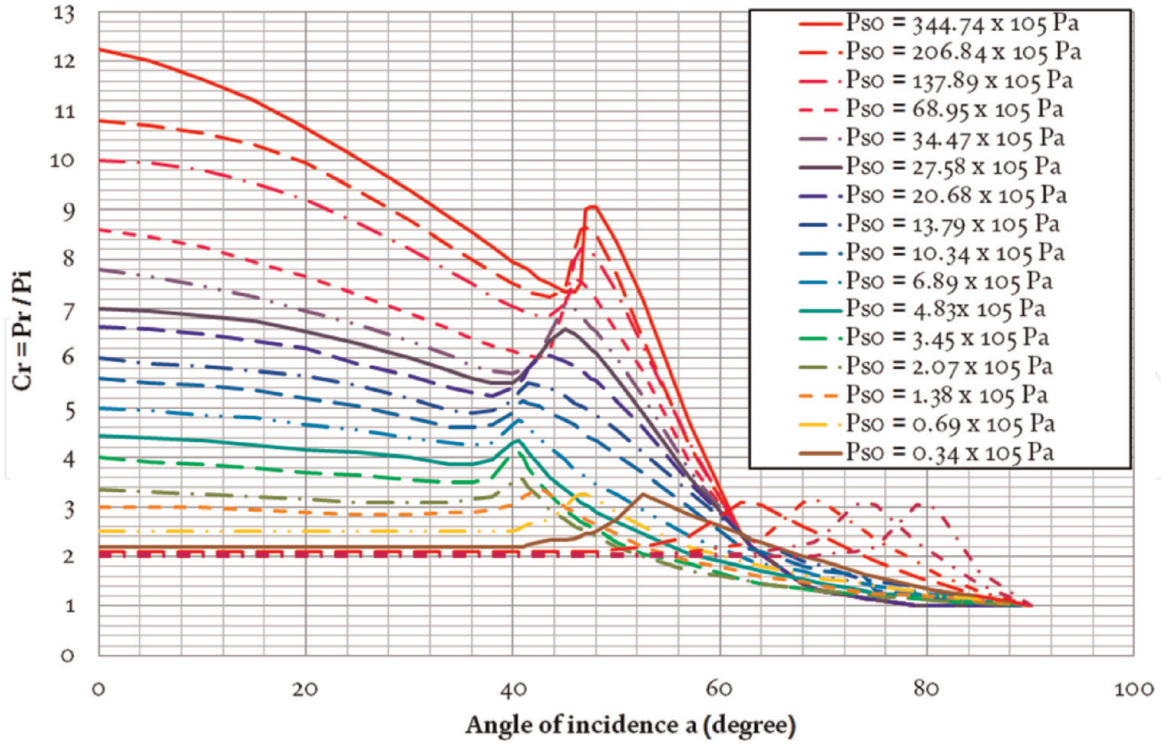
Figure 16.
Reflection coefficient angle of incidence and incident overpressure P_{so} (extracted from [30]).

Gauge	Z (m kg$^{1/3}$)	ΔP_i calculated (bar)	Cr abacus	ΔP_r (bar)	ΔP_r exp. (bar)	Deviation (%)
O	4.869	0.435	2.28	0.991	1.106	10.5
B	3.217	0.866	2.60	2.249	2.415	6.9
C	4.542	0.487	2.32	1.131	1.099	2.9
D	7.130	0.238	2.15	0.511	0.523	2.4

Table 4.
Comparison of reflected overpressures deduced from TNT abacus and measured.

The reflection coefficient is interpolated on the TNT abacus, and the reflected overpressure is deduced from $Cr = \frac{\Delta P_r}{\Delta P_i}$ and compared to the measurement. **Table 4** reports this analysis and demonstrates the validity of small-scale experiments. The maximum deviation is 10.5%.

The results presented here can be extrapolated by applying the Hopkinson law [31]. At scale 1, a shock wave results from the detonation of a mass of explosive M and impacts a point at a distance R from the center of the explosive charge. The shock wave arrives at a time Ta and is characterized by an overpressure ΔP^+, a positive and a negative impulse I^+ and I^-. The test is reproduced at scale k. Considering a mass of explosive kM, at a distance kR, the pressure profile presents the same overpressure ΔP, and the arrival time is multiplied by the scale factor k and hence the impulse kI^+ and kI^- too. Consequently, with this similitude law, the radial distance does not change with the scale:

$$Z = \frac{R}{M^{1/3}} = \frac{kR}{\left(k^3 M\right)^{1/3}} \tag{6}$$

The geometry of the target is also adapted by the scale factor k.

6. Conclusion

An experimental study of a pressure blast wave in a confined room facility was performed. The experiments were conducted at small scale with a gaseous charge. The facility simulated a single-story building with two rooms. The wall separating the two rooms was full or with an opening area. The effect of the location of this wall and the size of the opening were investigated. The pressure profile and the maximum overpressure were analyzed.

The pressure profiles are very complex to analyze. As expected, the overpressure increases with the confinement, and the protective effect of the wall decreases with the increasing size of the opening area. The most dangerous locations in terms of overpressure are at gauges J (ground level) and B (east wall) for all configurations due to their proximity to the explosive charge. In contrast, the least exposed zone corresponds to gauges G and F, which are the farthest from the charge but near a corner (for F) and near a wall (north) for G. Hence, the damage effects are severe since the maximum overpressure is never lower than 0.2 bar. The impulses were also examined, and values of 0.9 bar ms can be reached. The range of impulse level for the whole set of gauges and configurations is 0.3–0.6 bar ms. Severe damage results for high pressure and impulse.

Although this study is limited to a small scale and gaseous detonation charge, it is shown how the results can be applied at large scale and for a TNT charge. Numerical simulations would be interesting to complete this work.

Acknowledgements

Nomenclature

CE	center of explosion (of explosive charge)
Ci (i = 1, 2, 3 or 4)	configuration i (1, 2, 3 or 4)
C_r	reflection coefficient
$E_{P\text{-}TNT}$	TNT equivalency in terms of pressure
h	height
h_M	height of Mach stem
HOB	height of burst
k	scale factor
L	length
Lw	width
M	mass of the gaseous mixture
P_0	ambient pressure
P_r	absolute reflected pressure
R	radial distance
R_{conf}	confined radial distance
R_i	distance from the wall
R_{i0}	transition distance of formation
RR	receptor room
TR	transmitter room
$V_{RR\text{-}Ci}$	volume of receptor room in configuration i

$V_{TR\text{-}Ci}$	volume of transmitter room in configuration i
WF	full wall
WLO	wall with largest opening
WSO	wall with smallest opening
Z	scaled distance
Z_{conf}	confined scaled distance
Z_i (i = 1,2,3,4 or 5)	zone designation
Greek	
Δ_{max}	maximum angle of oblique reflection
ΔP^+	positive overpressure
ΔP_{FF}	positive overpressure in free field
ΔP_i or P_{s0}	incident overpressure
ΔP_{max}	maximum overpressure

Author details

Isabelle Sochet[1]*, Kevin Gault[1] and Luc Hakenholz[2]

1 INSA Centre Val de Loire, Université d'Orléans, Bourges, France

2 Direction Générale de l'Armement Techniques Navales, Toulon, France

*Address all correspondence to: isabelle.sochet@insa-cvl.fr

IntechOpen

References

[1] Weerheijm J, Van Wees RMM, Absil LHJ, De Bruyn PCAM, Karelse JW. The fireworks disaster in Enschede: Overview, reconstruction, safety and pyrotechnics. In: Proceedings of European Safety and reliability Conference (ESREL); Maastricht, The Netherlands; 2003. Vol. 2

[2] Willye RJ. West fertilizer company fire and explosion: A summary of the U. S. chemical safety and hazard investigation board report. Journal of Loss Prevention in the Process Industries. 2017;**49**:132-138

[3] Zhao B. Facts and lessons related to the explosion accident in Tianjin Port, China. Journal of the international society for the prevention and mitigation of natural hazards. 2016;**84**: 707-713

[4] ARIA. Feedback on Technological Accidents [Internet]. 2019. Available from: https://www.aria.developpement-durable.gouv.fr/?lang=en

[5] U.S. Department of the Army. Fundamentals of protective design for conventional weapons, Technical Manual 5855. 1986

[6] U.S. Department of the Army. Structures to resist the effects of accidental explosions, Technical Manual 5-1300. 1990

[7] Kinney GF, Graham KJ. Explosive Shocks in Air. Berlin Heidelberg: Springer-Verlag; 1985

[8] Remennikov AM. A review of methods for predicting bomb blast effects on buildings. Journal of Battlefield Technology. 2003;**6**:5-10

[9] Edri I, Savir Z, Feldgun VR, Karinski YS, Yankelevsky DZ. On blast pressure analysis due to a partially confined explosion: I. experimental studies. International Journal of Protective Structures. 2011;**2**:1-20

[10] Gebbeken N, Döge T. Explosion protection architectural design, urban planning and landscape planning. International Journal of Protective Structures. 2010;**1**:1-21

[11] Benselama A, Mame J-PWL, Monnoyer F. A 1D–3D mixed method for the numerical simulation of blast waves in confined geometries. Journal of Computational Physics. 2009;**228**: 6796-6810

[12] Reichenbach H, Neuwald P, Kuhl AL. Role of precision laboratory experiments in the understanding of large-scale blast phenomena. In: 17th International Symposium on Military Aspects of Blast and Shock (MABS), Julius J. Meszarus Lecture; Las Vegas, Nevada, USA; 2002

[13] Baker WE. Explosions in Air. Austin, TX and London, UK: University of Texas Press; 1973

[14] Ohrt A, Rogers J, Oliver C. Investigation of internal air blast propagation at small scale. In: 24th International Symposium on Military Aspects of Blast and Shock (MABS), Halifax, Canada; 2016

[15] Ram O, Nof E, Sadot O. Dependence of the blast load penetrating into a structure on initial conditions and internal geometry. Experimental Thermal and Fluid Science. 2016;**78**: 65-74

[16] Togashi F, Baum JD, Mestreau E, Löhner R, Sunshine D. Numerical simulation of long-duration blast wave evolution in confined facilities. Shock Waves. 2010;**20**:409-424. DOI: 10.1007/s00193-010-0278-7

[17] Milne AM, Cargil SB, Longbottom AW. Modelling of complex blast. International Journal of Protective Structure. 2016;**73**:325-339. DOI: 10.1177/2041419616661431

[18] Massoni J, Biamino L, Jourdan G, Houas L, Igra O. Experimental and numerical investigation of blast wave interaction with a three level building. Journal of Fluids Engineering. 2017; **139**(11):111106-111106-9. DOI: 10.1115/1.4037172

[19] Miura A, Mastuo A, Mizukaki T, Shiraishi T, Utsunomiya G, Takayama K, et al. Reflection and diffraction phenomena of blast wave propagation in nuclear fuel cycle facility. JSME International Journal Series B: Fluids and Thermal Engineering. 2004;**47**:287-292. DOI: 10.1299/jsmeb.47.287

[20] Jiang Z, Wang C, Miura Y, Takayama K. Three-dimensional propagation of the transmitted shock wave in a square cross-sectional chamber. Shock Waves. 2003;**13**:103-111. DOI: 10.1007/s00193-003-0197-y

[21] Binggeli E, Binggeli F, Schlapfer D, Bucher KM. Airblast predictions in tunnel/entrance configurations due to he-detonations near the tunnel portal. In: 13th International Symposium on Military Applications of Blast Simulation (MABS), The Hague, The Netherlands; 1993

[22] Rigas F, Sklavounos S. Experimentally validated 3-D simulation of shock waves generated by dense explosives in confined complex geometries. Journal of Hazardous Materials. 2005;**A121**:23-30

[23] Sauvan PE, Sochet I, Trélat S. Analysis of reflected blast wave pressure profiles in a confined room. Shock Waves. 2013;**22**:253-264

[24] Julien B, Sochet I, Vaillant T. Explosion in a multi-chamber: Experimental investigation. In: 22nd International Symposium on Military Aspects of Blast and Shock (MABS) Bourges, France; 2012

[25] Julien B, Sochet I, Vaillant T. Impact of the volume of rooms on shock wave propagation within a multi-chamber system. Shock Waves. 2016;**26**:87-108

[26] Sochet I, editor. Blast Effects-Physical Properties of Shock Waves. Series: Shock Wave and High Pressure Phenomena. Springer International Publishing AG; 2018

[27] Vanderstraeten B, Lefebvre M, Berghmans J. A simple blast wave model for bursting spheres based on numerical simulation. Journal of Hazardous Materials. 1996;**46**(2–3):145-157

[28] Rose TA, Smith PD. Oblique clearing: Blast loads on buildings at non-zero angles of incidence. In: 18th International Symposium on Military Aspects of Blast and Shock (MABS); Bad Reichenhall, Germany; 2004

[29] French Pyrotechnics Legislation [Internet]. 2019. Available from: https://www.legifrance.gouv.fr/affichTexte.do?cidTexte=JORFTEXT000000245167&categorieLien=cid

[30] U.S. Army Corps of Engineers, Naval Facilities Engineering Command, Air Force Civil Engineer Support Agency. Technical Manuals, Unified Facilities Criteria (UFC), Structures to resist the effects of accidental explosions, UFC 3-340-02, 2008

[31] Hopkinson B. British ordnance board minutes 13565. 1915